crystals

MDPI

Article

Ion-Track Template Synthesis and Characterization of $ZnSeO_3$ Nanocrystals

Alma Dauletbekova [1], Aiman Akylbekova [1], Gulnaz Sarsekhan [1], Abay Usseinov [1], Zein Baimukhanov [1], Artem Kozlovskiy [2], Liudmila A. Vlasukova [3], Fadey F. Komarov [3], Anatoli I. Popov [1,4,*] and Abdirash T. Akilbekov [1]

[1] Department of Technical Physics, L.N. Gumilyov Eurasian National University, Nur-Sultan 010008, Kazakhstan; alma_dauletbek@mail.ru (A.D.); aiman88_88@mail.ru (A.A.); gulnaz_sarsekhan@mail.ru (G.S.); usseinov_ab@enu.kz (A.U.); zein77@mail.ru (Z.B.); akilbekov_at@enu.kz (A.T.A.)
[2] Astana Branch of Institute of Nuclear Physics, Nur-Sultan 010008, Kazakhstan; kozlovskiy.a@inp.kz
[3] A.N. Sevchenko Institute of Applied Physical Problems, Belarusian State University, Kurchatov Street 5, 220045 Minsk, Belarus; vlasukova@mail.ru (L.A.V.); komarovf@bsu.by (F.F.K.)
[4] Institute of Solid State Physics, University of Latvia, 8 Kengaraga, LV-1063 Riga, Latvia
* Correspondence: popov@latnet.lv

Abstract: $ZnSeO_3$ nanocrystals with an orthorhombic structure were synthesized by electrochemical and chemical deposition into SiO_2/Si ion-track template formed by 200 MeV Xe ion irradiation with the fluence of 10^7 ions/cm^2. The lattice parameters determined by the X-ray diffraction and calculated by the CRYSTAL computer program package are very close to each other. It was found that $ZnSeO_3$ has a direct band gap of 3.8 eV at the Γ-point. The photoluminescence excited by photons at 300 nm has a low intensity, arising mainly due to zinc and oxygen vacancies. Photoluminescence excited by photons with a wavelength of 300 nm has a very low intensity, presumably due to electronic transitions of zinc and oxygen vacancies.

Keywords: SiO_2/Si track template; chemical and electrochemical deposition; $ZnSeO_3$ nanocrystals; XRD study; quantum chemical calculation

Citation: Dauletbekova, A.; Akylbekova, A.; Sarsekhan, G.; Usseinov, A.; Baimukhanov, Z.; Kozlovskiy, A.; Vlasukova, L.A.; Komarov, F.F.; Popov, A.I.; Akilbekov, A.T. Ion-Track Template Synthesis and Characterization of $ZnSeO_3$ Nanocrystals. *Crystals* **2022**, *12*, 817. https://doi.org/10.3390/cryst12060817

Academic Editors: Fu-Der Lai, Mu-Chun Wang and Wen-Ching Hsieh

Received: 28 February 2022
Accepted: 6 June 2022
Published: 9 June 2022

1. Introduction

Quite a lot of time passed from the time of the first observation of ion tracks to their application in various technological developments [1–3]. It should be noted that only the use of high-energy ion accelerators made it possible to provide that huge breakthrough in the development of the application and use of various ion-track technologies [4–9]. Now that high-energy ion accelerator systems are available, a large number of such fundamentally new experimental studies can be carried out [10–20].

Among these experiments, the targeted use of ion irradiation to form new nanostructured materials such as nanoclusters and nanowires should be noted, which have received particularly great attention in the last twenty years due to their special physical properties and new applications [21,22]. It is important to mention here that the so-called ion-track template synthesis is one of the simplest and most inexpensive methods for obtaining metal and semiconductor nanoclusters and nanowires [23–33]. The "ion-track etching" technique is a quite industrial method that can be used to create nanoscale pores in a range of different materials, including polymers, semiconductors, and dielectrics. Among them, SiO_2 and Si_3N_4, which are commonly used in semiconductor processing. Such nanoporous materials could be used as templates for nanowire and nanotube synthesis. Etched pores could be filled with various materials using the methods of chemical or electrochemical deposition. As shown in the Table 1, different ensembles of CdTe nanocrystals, CdO and other binary compounds, as well as wide-gap semiconductor oxides, such as ZnO, were successfully formed by this method in SiO_2/Si ion-track templates.

Table 1. Examples of nanostructures obtained by ion-track template synthesis in SiO_2/Si track templates.

No.	Type of Nanostructure	Method	References
1	ZnO nanocrystals with structures of sphalerite, wurtzite, and rock salt	Electrodeposition	[34,35]
2	CdTe nanocrystals	Electrodeposition, chemical deposition. Photoelectrochemical deposition	[36–38]
3	PbSe nanocrystals	Photoelectrochemical deposition	[39]
3	CdO nanocrystals	Chemical deposition	[37]
4	$ZnSe_2O_5$ nanocrystals	Electrodeposition	[40,41]
5	$ZnSeO_3$ nanocrystals	Electrodeposition	present work
6	Cu and Ni nanocrystals	Electrodeposition	[42]
7	Layers of metallic Cu and Ni	Electrodeposition	[43]
8	Ag dendrites	Chemical deposition	[44]
9	Au nanostructures	Chemical deposition	[45]

Among them, zinc oxide occupies a very special place. ZnO-based materials can be used as optoelectronic transducers, fluorescent materials, gas-sensor elements, and biological sensors, catalysts, X-ray, and gamma radiation detectors [46–56]. These applications of ZnO are usually considered for its crystalline wurtzite (WS) phase. This is because under normal conditions, ZnO has the crystal structure of wurtzite. Possible applications of various structural modifications of ZnO crystal in semiconductor technology are described in [46,53,55–60]. The high symmetry of the crystal structure allows us to expect some advantages, such as lower carrier scattering, higher doping efficiency, etc., which can be used in various devices, such as radiation detectors [34,35,46].

From the point of view of obtaining new promising materials for optoelectronics, nanoelectronics, and sensorics, a detailed study of nanomaterials based on other complex zinc-based oxides obtained in SiO_2/Si templates is of undoubted interest. Therefore, a logical continuation of the work in [40,41], where the results of the synthesis of $ZnSe_2O_5$ were reported, is the synthesis and characterization of similar but simpler nanocrystals of $ZnSeO_3$, also obtained in SiO_2/Si templates. Note that although in recent years several successful attempts have been made to synthesize various types of thin films and nanostructures based on $ZnSeO_3$ [61–63], this work is the first demonstration of the possibility of their synthesis in SiO_2/Si templates.

2. Experimental

2.1. Fabrication of Track Templates and Template Synthesis

The SiO_2/Si structure was prepared by thermal oxidation of a silicon substrate (n- or p-type Si) in a wet oxygen atmosphere at 900 °C. The thickness of the silicon dioxide layer according to ellipsometry was 700 nm.

Earlier, in [64,65], the simulation of track formation processes in SiO_2/Si structures was performed, as well as a comparison with experimental data. It was found that latent tracks could be created in SiO_2 film via irradiation with ^{84}Kr or ^{132}Xe ions if specific ionization energy losses of these species were exceeding the threshold value. In our experiment, SiO_2/Si structures were irradiated with 200 MeV ^{132}Xe ions to fluences of 10^7–10^8 ions/cm^2. At such small fluences, there are no tracks overlapping, and the background of radiation defects introduced during irradiation is insignificant.

Chemical etching of the ion-irradiated SiO_2/Si structures was carried out in a 4% aqueous solution of HF with the addition of palladium (m (Pd) = 0.025 g) at 25 ± 1 °C. Before and after etching, the samples were subjected to ultrasonic cleaning of the surface.

Template synthesis was carried out using chemical deposition (CD) and electrodeposition (ECD). The aqueous solution prepared from $ZnSO_4$ (7.2 g/L) and SeO_2 (0.2 g/L) was used for CD. The precipitation times were 15, 20, and 25 min, and the precipitation temperature was 20 °C. The same aqueous solution of $ZnSO_4$ and SeO_2 was used as an electrolyte for ECD, too. The deposition of nanoprecipitates was carried out for 7 min at 50 °C in the potentiostatic mode at voltages of 1.5 and 1.75 V.

2.2. Diagnostics of SiO_2/Si Templates with Deposited Nanoprecipitates

The morphology of the etched nanoporous SiO_2/Si samples as well as the templates with nanoprecipitates was investigated using a scanning electron microscope (SEM), JSM-7500F. The crystallographic structure of the precipitates was investigated by X-ray diffraction (XRD). XRD patterns were obtained using the X-ray diffractometer D8 ADVANCE ECO with Cu-anode comprised between angles of 2θ 30° and 110° in increments of 0.01°. The software Bruker AXSDIFFRAC.EVAv.4.2 and the international ICDD PDF-2 database were used to identify the phases and study the crystal structure of Zn-based precipitates.

The photoluminescence (PL) spectra were recorded at room temperature using an Agilent Technologies spectrofluorimeter (Cary Eclipse Fluorescence Spectrophotometer, Santa Clara, CA, USA) in a spectral range from 300 to 800 nm at 300 nm excitation.

The HP 66312A current source and the 34401A Agilent (Santa Clara, CA, USA) multimeter were used to measure the electrical properties of created templates with nanoprecipitates. Current–voltage characteristics (CVC) were taken from the area of filled nanochannels of 0.3 cm^2. The scheme of installation for CVC measuring was as follows: A sample with deposited nanoprecipitates was placed between two metal plates which overlapped only at the area of sample with nanochannels. The plates were then connected to the current source in series connection of the multimeter. All CVCs were performed using a second-order polynomial fitting.

3. Results and Discussion

SEM and XRD Analysis of Deposited Samples

SEM analysis of nanopores after etching and nanoprecipitates' deposition allows to control the size, shape, and "filling in" of nanopores. Figure 1 shows SEM images of the templates after CD.

As the SEM images' analysis showed, most of the template pores were filled after CD for 15 min (the filling degree was 89.5%), and the filling degree was 51.3% and 40.2% after CD for 20 and 25 min, respectively. With increasing the deposition time, a protrusion of the deposited substance from the nanopores at the surface was clearly observed (Figure 1).

XRD patterns of the samples after chemical deposition are shown in Figure 2. The corresponding crystallographic parameters of nanoprecipitates in ion-track templates calculated from XRD data are summarized in Table 2. For XRD peak assignment of orthorhombic $ZnSeO_3$, the JCPDS-78-0446 pattern was used.

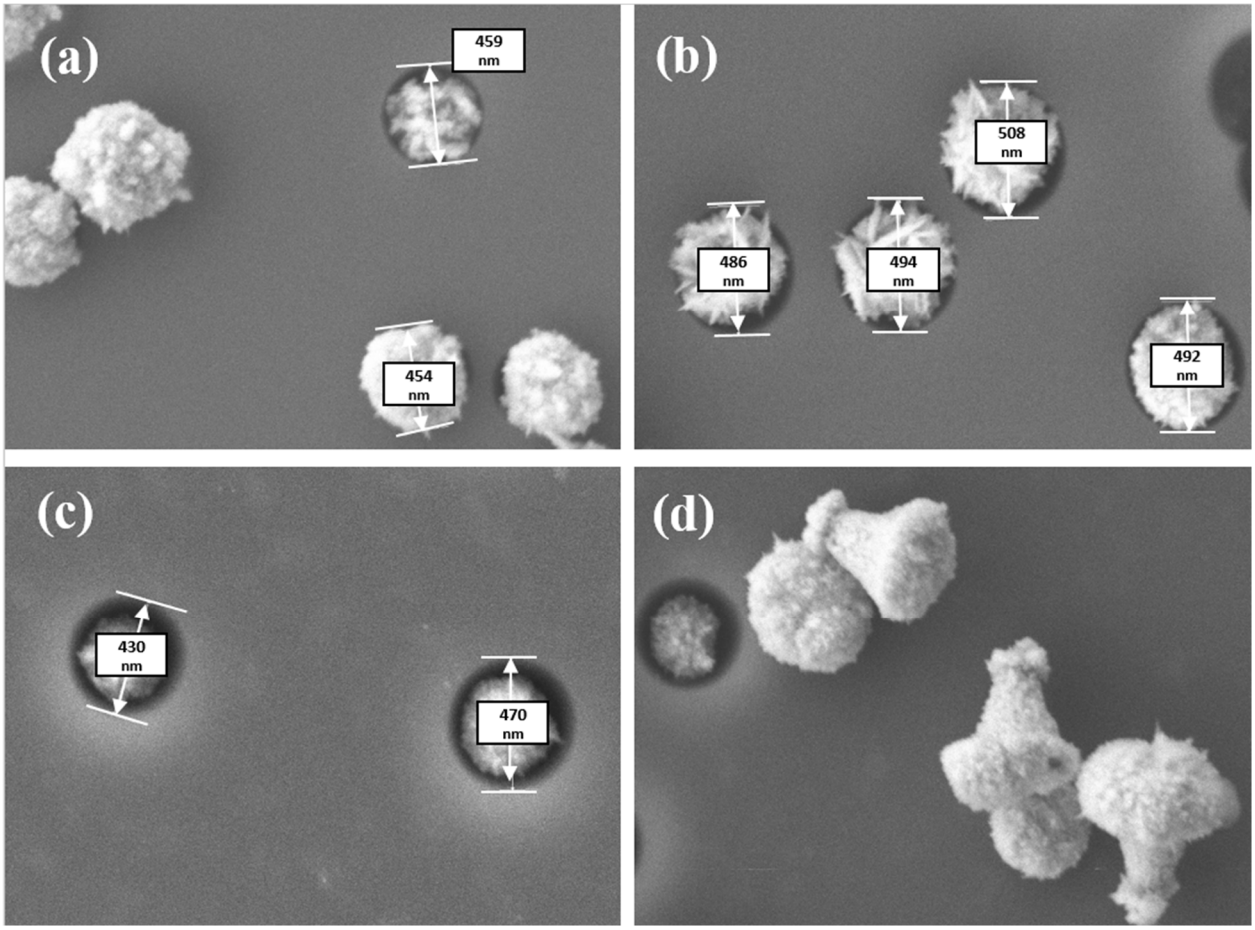

Figure 1. SEM images of pore-filling after 15 min CD (**a**), 20 min CD (**b**), and 25 min CD (**c**), and obtained nanostructures formed on the surface (**d**). The pore diameter varied from 400 to 500 nm.

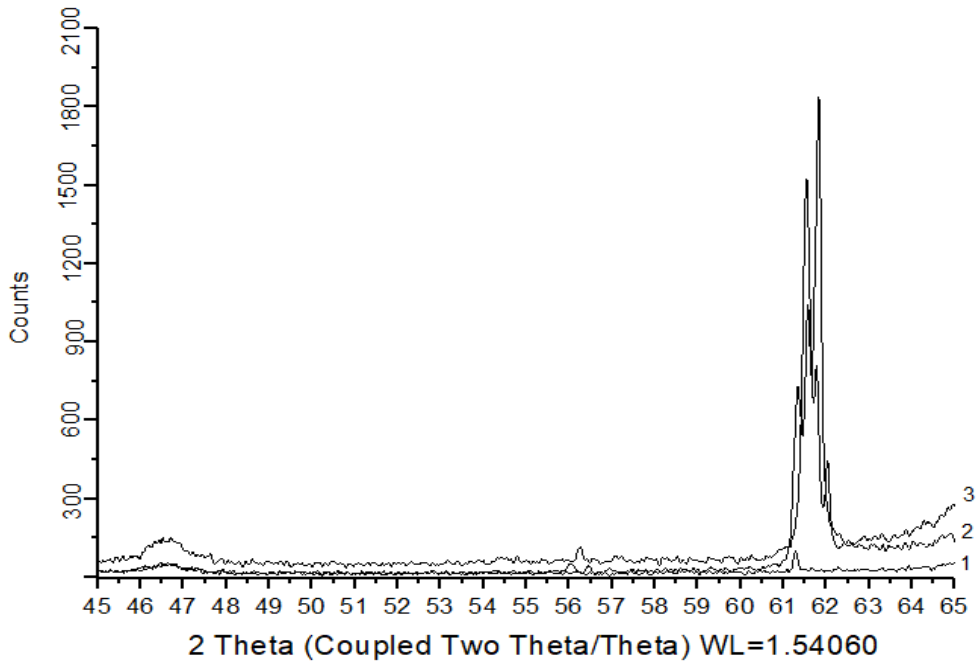

Figure 2. XRD patterns of the templates with nanoprecipitates formed by chemical deposition: the deposition duration was 15 min (1), 20 min (2), and 25 min (3).

Table 2. Crystallographic parameters of $ZnSeO_3$ nanoprecipitates in SiO_2/Si templates calculated from XRD data.

No.	2θ°	hkl	d, Å	The Size of Crystallites L, nm	Cell Parameters, Å	FWHM	Density ρ, (g/cm^3)
1	46.38	241	1.956	12.1	5.9231 7.6652 5.0400	1.11	5.584
2	46.67 56.27 61.54	241 341 350	1.945 1.6335 1.50561	70.3	5.9231 7.6652 5.0400	0.94 0.11 0.180	5.584
3	46.66 56.00 61.33	241 341 350	1.945 1.6406 1.5103	84.82	5.8640 7.5767 5.0026	0.95 0.14 0.16	5.588

Analysis of XRD data for the samples obtained by CD showed the formation of $ZnSeO_3$ nanocrystals with an orthorhombic crystal structure and the space group Pnma (see Figure 2 and Table 2).

Figure 3 shows SEM images of the surface after ED. One can see that the level of pore filling was substantially lower in comparison with the samples formed by chemical deposition. Therefore, the pore-filling degree was only 10% if the precipitate deposition was carried out at a voltage of 1.5 V, and 16% if the deposition was carried out at a voltage of 1.75 V. Possibly, it is necessary to increase the deposition voltage to achieve complete filling of nanopores. This is a subject for future experiments.

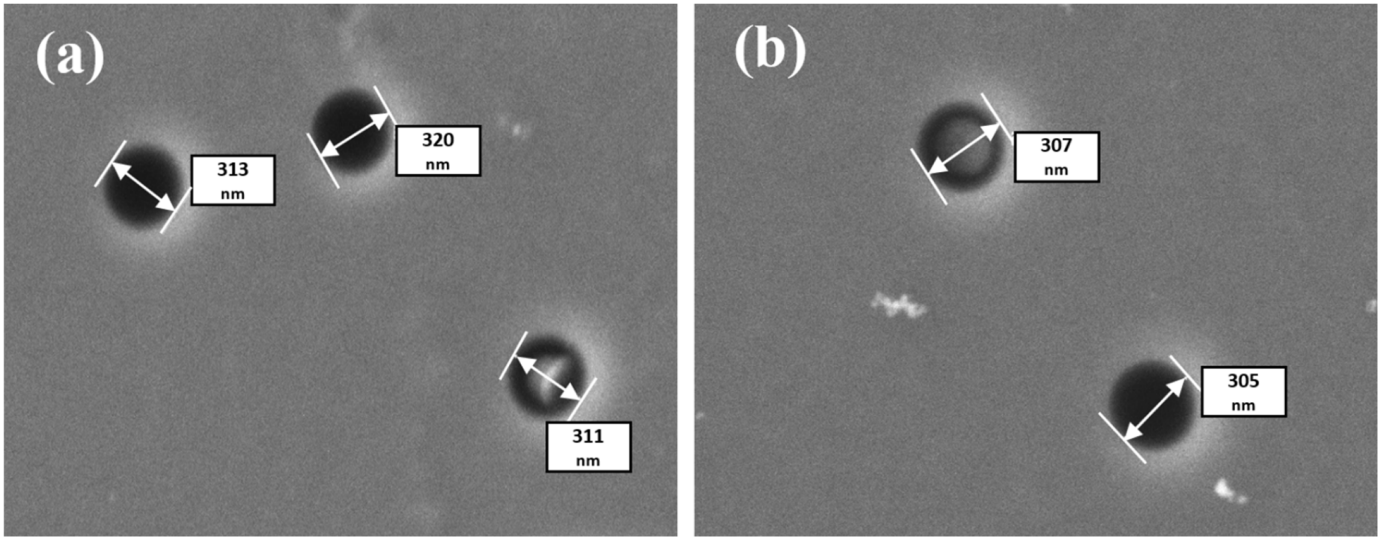

Figure 3. SEM images of the pores after ED with different voltages: (**a**) U = 1.5 V and (**b**) U = 1.75 V. Pore diameter ~300 nm.

Figure 4 shows the diffractograms after ED, while XRD analysis results were collect in Table 3.

Thus, the synthesing $ZnSeO_3$ nanocrystals inside nanopores belong to orthorhombic structure with space group Pnma was established.

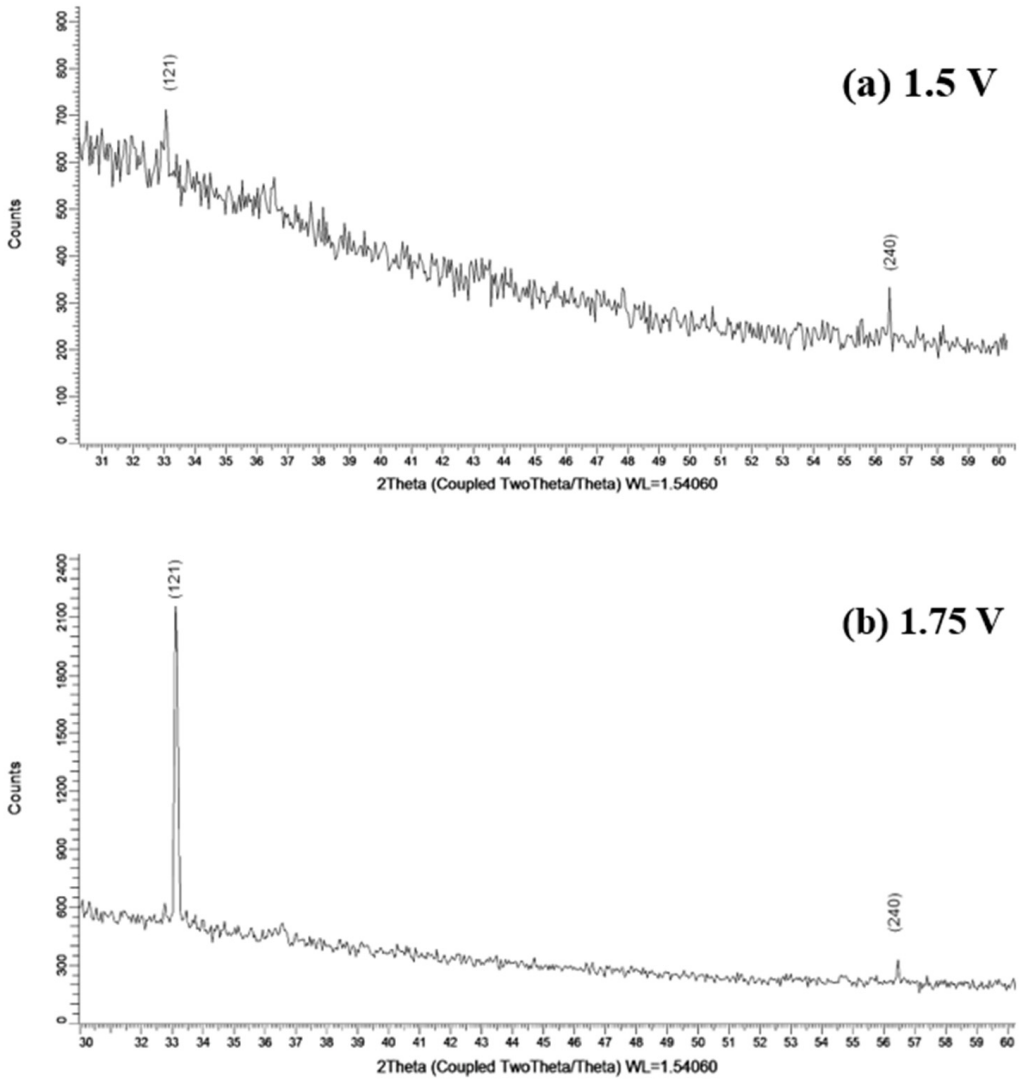

Figure 4. XRD after ED at 1.5 V (**a**) and 1.75 V (**b**).

Table 3. XRD results of ED samples.

ED at 1.5 V					
(hkl)	**2θ°**	**d, Å**	**L, nm**	**Cell Parameters, Å**	**Degree of Crystallinity**
121 240	33.060 56.432	2.70738 1.62924	54.89 164.17	a = 5.94052, b = 7.66370 c = 5.06273	68.5%
ED at 1.75 V					
121 240	33.137 56.470	2.70130 1.62823	74.04 155.56	a = 5.92538, b = 7.60209 c = 5.04784	70.8%

4. $ZnSeO_3/SiO_2/Si$ Photoluminescence and Current–Voltage Characteristic

The photoluminescence (PL) spectra were recorded, using an Agilent Technologies spectrofluorimeter (Cary Eclipse Fluorescence Spectrophotometer), in the spectral range from 300 to 800 nm at room temperature at 300 nm excitation.

The PL spectra of $ZnSeO_3/SiO_2/Si$ present a wide band from 400 to 600 nm, as in the case of ED synthesized $ZnSe_2O_5/SiO_2/Si$ [40]. The luminescence of $ZnSe_2O_3$ can be expected, as for $ZnSe_2O_5$, as a combination of zinc oxide and zinc selenide luminescence.

Similar to ZnO [66], the PL spectrum contains luminescence sub-bands of zinc vacancies (V_{Zn}, 2.94 eV) and oxygen vacancies (V_O). The bands observed in the PL spectrum in the region 2.1 eV are similar to the PL band observed in ZnSe. This band is attributed by the authors of [67] to a complex center consisting of a zinc vacancy and an impurity small donor: V_{Zn} + D. As follows from Figure 5, the luminescence spectrum is quite complex and consists of several components. Similar, though not so complicated spectra are also observed in ZnO [47,66] and ZnSe [67,68]. A more accurate analysis of the excitation spectra of individual luminescence bands will make it possible to more accurately decipher their origin. However, this is beyond the scope of this work, but one subsequent article will be devoted to this. We only note here that the complex nature of the luminescence spectrum may also reflect the presence of a certain number of anti-site defects.

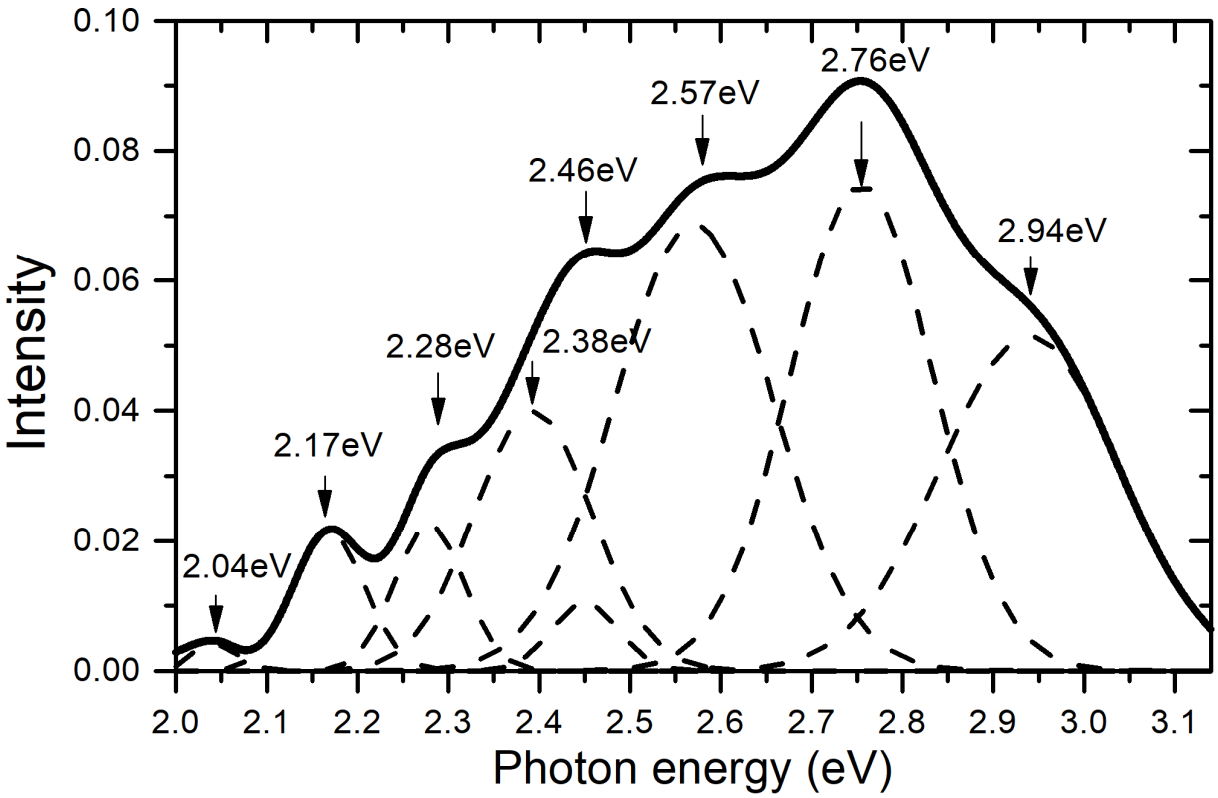

Figure 5. Differential PL spectra of $ZnSeO_3/SiO_2/Si$ after CD for 15 min, with Gaussian curves.

The appropriate current–voltage characteristics (CVC) obtained for $ZnSeO_3/SiO_2/Si$ are presented in Figure 6. The HP 66312A current source and the 34401A Agilent (Santa Clara, CA, USA) multimeter were used to measure their electrical properties. Current–voltage characteristics (CVC) were taken from an array of filled nanochannels of 0.3 cm^2. The scheme of installation for CVC measurement is as follows: The sample with deposited nanoprecipitates was placed between two metal plates, and the plates overlap only the part where nanochannels are. The plates were then connected to the current source in series connection of the multimeter. All CVCs were performed using a second-order polynomial fitting.

In the structure of $ZnSeO_3/SiO_2/Si$, the Si substrate has n-type conductivity. From the CVC analysis of the obtained CdTe (WZ NCs)/SiO_2/Si structure [36], it can be argued that this structure shows an electronic type of conductivity.

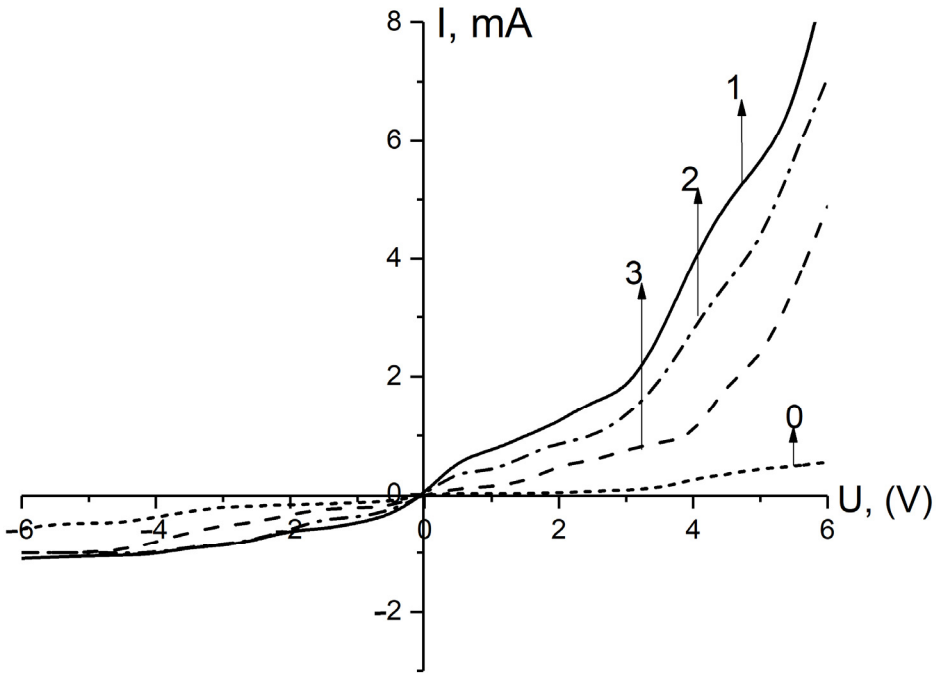

Figure 6. CVC of $ZnSeO_3$ after CD: 0—SiO_2/Si; 1—after 15 min of deposition; 2—after 20 min; 3—after 25 min.

5. Computer Modeling of $ZnSeO_3$

We also performed non-empirical calculations of the $ZnSeO_3$ crystal in the approximation of linear combinations of atomic orbitals (LCAO) using the exchange–correlation functional within general gradient approximation (GGA) [69]. The calculations were performed in the CRYSTAL program [70]. To describe the atoms of $ZnSeO_3$ crystal, the following Gauss-type function basic sets were chosen: the Jaffe basis [71] was used for the zinc (Zn) and oxygen (O) atoms, and the Towler basis [72] for the selenium (Se) atom. To better describe both the structural and electronic properties, the last sp-orbital from the original Se basis was removed.

It is known that for a better description of the electronic structure of a crystal, it is necessary to accurately determine the total energy of the crystal cell [73,74]. From a well-known theory, the calculation of total energy within a periodic model of crystal is not straightforward [70]. Due to this reason, in the CRYSTAL program, a complex scheme of preliminary analysis and subsequent calculation of crystalline integrals was introduced. In our calculations, high convergence tolerances for the Coulomb and exchange integrals have been chosen for the Coulomb overlap (10^{-7}), Coulomb penetration (10^{-7}), exchange overlap (10^{-7}), first exchange pseudo-overlap (10^{-7}), and the second exchange pseudo-overlap (10^{-14}). These tolerances mean that the values of the atomic orbitals overlap, and if these values are greater than those specified in the calculation, then the Coulomb and exchange integrals are calculated exactly, otherwise they are neglected or calculated approximately.

The effective atomic charges and bond population were calculated using the Mulliken analysis [75].

We used a periodic model of a primitive $ZnSeO_3$ cell, consisting of 56 atoms (Figure 7). The calculated lattice parameters (a, b, c), crystal density (ρ_V), and effective atomic charges (q_{eff}) are presented in Table 4, together with experimental results.

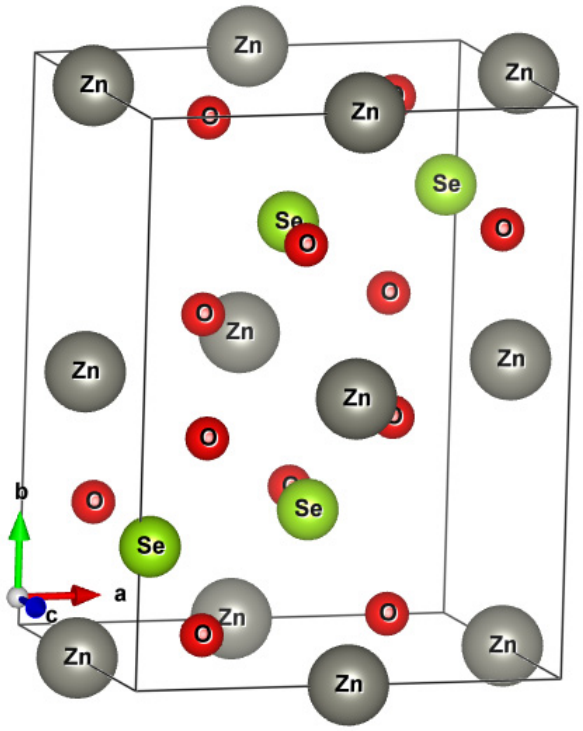

Figure 7. Atomic structure of $ZnSeO_3$ unit cell (56 atoms). The boundaries of the cell and the directions of the translation vectors are shown.

Table 4. Calculated parameters of $ZnSeO_3$ crystal.

Parameter	This Work, Calc.	This Work, Exper.	Exper. [76]
a, Å	5.85	5.90	5.92
b, Å	7.69	7.75	7.66
c, Å	5.19	5.04	5.04
ρ_V (g/cm^3)	5.44	5.58	-
q_{eff} (Zn/Se/O)	+1.16/+1.36/−0.84	-	-

We are plotted the band structure at the highly symmetric points of the Brillouin zone and along directions between them, together with the density of the electronic states as shown Figure 8. The maximum of the valence band appeared near the Y-point, while the conduction band minimum occurred at T-point, showing the indirect character of the band structure. The calculated band gap was 3.8 eV. Additionally, as shown by the density of electronic states, the top of valence band was represented mainly by O 2p states, while the bottom of conduction band and levels above the bottom are consisted from Se 3d, 4s and Zn 3d, 4s states, respectively. Thus, it can be claim that we have typical ionic compounds, although subsequent charge distribution analysis showed significant covalent contribution to chemical bounds of the crystal.

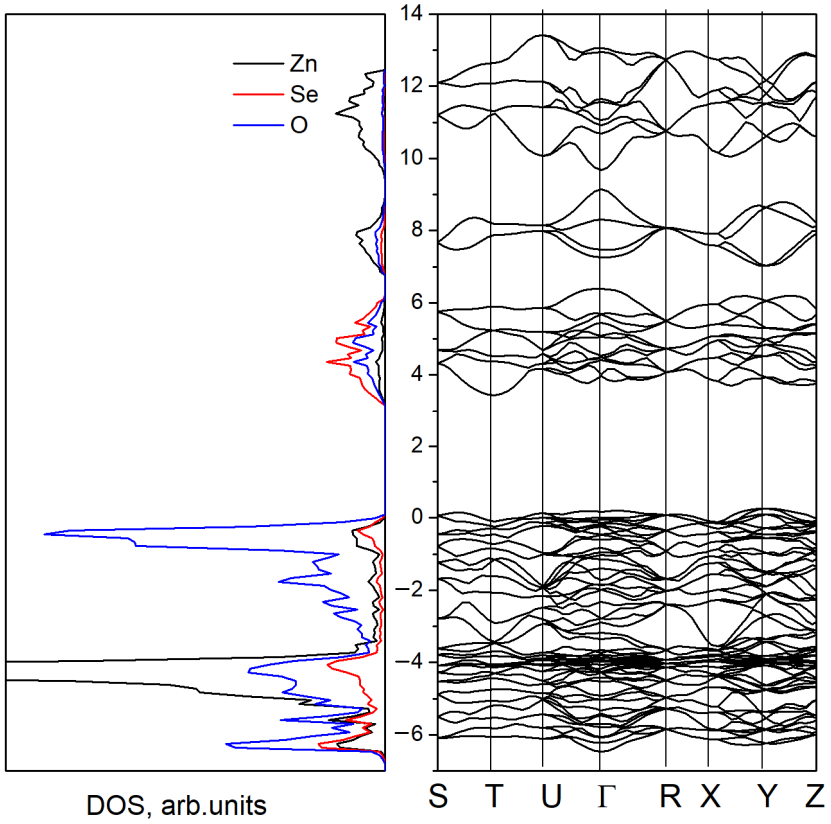

Figure 8. Density of states and band structure of pure $ZnSeO_3$ crystal.

6. Conclusions

$ZnSeO_3$ nanocrystals were synthesized and studied for the first time. The nanocrystals were obtained by chemical and electrochemical deposition into a track-template matrix. Crystal structure and phase composition were studied by XRD. The crystalline phase of all samples was the same: an orthorhombic structure, with almost identical unit cell parameters. The method of CD was more effective in obtaining this crystal compared to the method of ED. The application of the CD method affords the possibility to fill practically all nanopores, and thus it is a more convenient and accessible technique. Computer simulations showed that $ZnSeO_3$ is a direct-gap semiconductor with E_g = 3.8 eV. The PL spectra at room temperature showed a wide emission band in the spectral range of 400–600 nm. The PL band was caused mainly by zinc and oxygen vacancies.

Author Contributions: Conceptualization, A.D., A.A., A.T.A., A.U. and A.I.P., formal analysis, A.A., G.S., Z.B. and A.K.; writing—original draft preparation, A.D., A.A., A.U., F.F.K. and L.A.V.; writing—review and editing, A.A., A.U. and A.I.P.; visualization, A.K., A.D., A.A. and A.U.; project administration, A.D.; funding acquisition, A.D. and A.I.P. All authors have read and agreed to the published version of the manuscript.

Funding: The work was carried out within the framework of the grant AP05134367 of the Ministry of Education and Science of the Republic of Kazakhstan.

Institutional Review Board Statement: Not applicable.

Informed Consent Statement: Not applicable.

Data Availability Statement: The data presented in this study are available on request from the corresponding author. The data are not publicly available due to the ongoing research.

Acknowledgments: A.I.P. thanks the Institute of Solid-State Physics, University of Latvia. ISSP UL as the Center of Excellence is supported through the Framework Program for European universities, Union Horizon 2020, H2020-WIDESPREAD-01–2016–2017-TeamingPhase2, under Grant Agreement No. 739508, CAMART2 project.

Conflicts of Interest: The authors declare no conflict of interest.

References

1. Williams, J.S. Materials modification with ion beams. *Rep. Prog. Phys.* **1986**, *49*, 491–587. [CrossRef]
2. Lang, M.; Tracy, C.L.; Palomares, R.I.; Zhang, F.; Severin, D.; Bender, M.; Trautmann, C.; Park, C.; Prakapenka, V.B.; Skuratov, V.A.; et al. Characterization of ion-induced radiation effects in nuclear materials using synchrotron X-ray techniques. *J. Mater. Res.* **2015**, *30*, 1366–1379. [CrossRef]
3. Jain, I.P.; Agarwal, G. Ion beam induced surface and interface engineering. *Surf. Sci. Rep.* **2011**, *66*, 77–172. [CrossRef]
4. Popov, A.; Lushchik, A.; Shablonin, E.; Vasil'Chenko, E.; Kotomin, E.; Moskina, A.; Kuzovkov, V. Comparison of the F-type center thermal annealing in heavy-ion and neutron irradiated Al_2O_3 single crystals. *Nucl. Instrum. Methods Phys. Res. Sect. B Beam Interact. Mater. At.* **2018**, *433*, 93–97. [CrossRef]
5. Tanaka, A. Multiple Applications of Ion Beams in Life Science. *Quantum Beam Sci.* **2019**, *3*, 19. [CrossRef]
6. Zhong, Y.; Dai, Y.; Shi, F.; Song, C.; Tian, Y.; Lin, Z.; Zhang, W.; Shen, Y. Effects of Ion Beam Etching on the Nanoscale Damage Precursor Evolution of Fused Silica. *Materials* **2020**, *13*, 1294. [CrossRef]
7. van Vuuren, A.J.; Ibrayeva, A.D.; O'Connell, J.H.; Skuratov, V.A.; Mutali, A.; Zdorovets, M.V. Latent ion tracks in amorphous and radiation amorphized silicon nitride. *Nucl. Instrum. Methods Phys. Res. Sect. B* **2020**, *473*, 16–23. [CrossRef]
8. Wen, Q.; Wei, X.; Jiang, F.; Lu, J.; Xu, X. Focused Ion Beam Milling of Single-Crystal Sapphire with A-, C-, and M-Orientations. *Materials* **2020**, *13*, 2871. [CrossRef]
9. Kim, C.; Ahn, S.; Jang, D. Review: Developments in micro/nanoscale fabrication by focused ion beams. *Vacuum* **2012**, *86*, 1014–1035. [CrossRef]
10. Córdoba, R. Editorial for the Special Issue on Nanofabrication with Focused Electron/Ion Beam Induced Processing. *Micromachines* **2021**, *12*, 893. [CrossRef]
11. Kimura, K.; Sharma, S.; Popov, A. Fast electron–hole plasma luminescence from track-cores in heavy-ion irradiated wide-band-gap crystals. *Nucl. Instrum. Methods Phys. Res. B* **2002**, *191*, 48–53. [CrossRef]
12. Schwartz, K.; Sorokin, M.V.; Lushchik, A.; Lushchik, C.; Vasil, E.; Papaleo, R.M.; Trautmann, C. Color center creation in LiF crystals irradiated with 5-and 10-MeV Au ions. *Nucl. Instrum. Methods Phys. Res. B* **2008**, *266*, 2736–2740. [CrossRef]
13. Belianinov, A.; Burch, M.J.; Ievlev, A.; Kim, S.; Stanford, M.G.; Mahady, K.; Lewis, B.B.; Fowlkes, J.D.; Rack, P.D.; Ovchinnikova, O.S. Direct Write of 3D Nanoscale Mesh Objects with Platinum Precursor via Focused Helium Ion Beam Induced Deposition. *Micromachines* **2020**, *11*, 527. [CrossRef] [PubMed]
14. Kotomin, E.A.; Kuzovkov, V.N.; Popov, A.I.; Vila, R. Kinetics of F center annealing and colloid formation in Al_2O_3. *Nucl. Instrum. Methods Phys. Res. B* **2016**, *374*, 107–110. [CrossRef]
15. Hari, S.; Trompenaars, P.H.F.; Mulders, J.J.L.; Kruit, P.; Hagen, C.W. Combined Focused Electron Beam-Induced Deposition and Etching for the Patterning of Dense Lines without Interconnecting Material. *Micromachines* **2021**, *12*, 8. [CrossRef]
16. Tomić Luketić, K.; Karlušić, M.; Gajović, A.; Fazinić, S.; O'Connell, J.H.; Pielić, B.; Radatović, B.; Kralj, M. Investigation of Ion Irradiation Effects in Silicon and Graphite Produced by 23 MeV I Beam. *Materials* **2021**, *14*, 1904. [CrossRef]
17. Kotomin, E.; Kuzovkov, V.; Popov, A.I.; Maier, J.; Vila, R. Anomalous kinetics of diffusion-controlled defect annealing in irradiated ionic solids. *J. Phys. Chem. A* **2018**, *122*, 28–32. [CrossRef]
18. Crespillo, M.L.; Graham, J.T.; Agulló-López, F.; Zhang, Y.; Weber, W.J. Real-Time Identification of Oxygen Vacancy Centers in $LiNbO_3$ and $SrTiO_3$ during Irradiation with High Energy Particles. *Crystals* **2021**, *11*, 315. [CrossRef]
19. Lushchik, A.; Feldbach, E.; Kotomin, E.A.; Kudryavtseva, I.; Kuzovkov, V.N.; Popov, A.I.; Seeman, V.; Shablonin, E. Distinctive features of diffusion-controlled radiation defect recombination in stoichiometric magnesium aluminate spinel single crystals and transparent polycrystalline ceramics. *Sci. Rep.* **2020**, *10*, 7820.
20. Laptev, R.; Svyatkin, L.; Krotkevich, D.; Stepanova, E.; Pushilina, N.; Lomygin, A.; Ognev, S.; Siemek, K.; Uglov, V. First-Principles Calculations and Experimental Study of H+-Irradiated Zr/Nb Nanoscale Multilayer System. *Metals* **2021**, *11*, 627. [CrossRef]
21. Lorenz, M.; Rao, M.S.R.; Venkatesan, T.; Fortunato, E.; Barquinha, P.; Branquinho, R.; Salgueiro, D.; Martins, R.; Carlos, E.; Liu, A.; et al. The 2016 oxide electronic materials and oxide interfaces roadmap. *J. Phys. D Appl. Phys.* **2016**, *49*, 433001. [CrossRef]
22. Coll, M.; Fontcuberta, J.; Althammer, M.; Bibes, M.; Boschker, H.; Calleja, A.; Cheng, G.; Cuoco, M.; Dittmann, R.; Dkhil, B.; et al. Towards oxide electronics: A roadmap. *Appl. Surf. Sci.* **2019**, *482*, 433001. [CrossRef]
23. Toimil-Molares, M.E. Characterization and properties of micro-and nanowires of controlled size, composition, and geometry fabricated by electrodeposition and ion-track technology. *Beilstein J. Nanotechnol.* **2012**, *3*, 860–883. [CrossRef] [PubMed]
24. Mo, D.; Liu, J.; Yao, H.; Duan, J.; Hou, M.; Sun, Y.; Chen, Y.; Xue, Z.; Zhang, L. Preparation and characterization of CdS nanotubes and nanowires by electrochemical synthesis in ion-track templates. *J. Cryst. Growth* **2008**, *310*, 612–616. [CrossRef]

25. Ulrich, N.; Spende, A.; Burr, L.; Sobel, N.; Schubert, I.; Hess, C.; Trautmann, C.; Toimil-Molares, M.E. Conical Nanotubes Synthesized by Atomic Layer Deposition of Al_2O_3, TiO_2, and SiO_2 in Etched Ion-Track Nanochannels. *Nanomaterials* **2021**, *11*, 1874. [CrossRef] [PubMed]
26. Spende, A.; Sobel, N.; Lukas, M.; Zierold, R.; Riedl, J.C.; Gura, L.; Schubert, I.; Moreno, J.M.M.; Nielsch, K.; Stühn, B.; et al. TiO_2, SiO_2, and Al_2O_3 coated nanopores and nanotubes produced by ALD in etched ion-track membranes for transport measurements. *Nanotechnology* **2015**, *26*, 335301. [CrossRef]
27. Sobel, N.; Hess, C.; Lukas, M.; Spende, A.; Stühn, B.; Toimil-Molares, M.E.; Trautmann, C. Conformal SiO_2 coating of sub-100 nm diameter channels of polycarbonate etched ion-track channels by atomic layer deposition. *Beilstein J. Nanotechnol.* **2015**, *6*, 472–479. [CrossRef]
28. Panina, L.V.; Zagorskiy, D.L.; Shymskaya, A.; Doludenko, I.M.; Evstigneeva, S.A.; Melnikova, P.D.; Gilimyanova, A.R. 1D Nanomaterials in Fe-Group Metals Obtained by Synthesis in the Pores of Polymer Templates: Correlation of Structure, Magnetic, and Transport Properties. *Phys. Status Solidi A* **2022**, *219*, 2100538. [CrossRef]
29. Dutt, S.; Apel, P.; Lizunov, N.; Notthoff, C.; Wen, Q.; Trautmann, C.; Mota-Santiago, P.; Kirby, N.; Kluth, P. Shape of nanopores in track-etched polycarbonate membranes. *J. Membr. Sci.* **2021**, *638*, 119681. [CrossRef]
30. Zagorskiy, D.; Doludenko, I.; Zhigalina, O.; Khmelenin, D.; Kanevskiy, V. Formation of Nanowires of Various Types in the Process of Galvanic Deposition of Iron Group Metals into the Pores of a Track Membrane. *Membranes* **2022**, *12*, 195. [CrossRef]
31. Blonskaya, I.; Lizunov, N.; Olejniczak, K.; Orelovich, O.; Yamauchi, Y.; Toimil-Molares, M.; Trautmann, C.; Apel, P. Elucidating the roles of diffusion and osmotic flow in controlling the geometry of nanochannels in asymmetric track-etched membranes. *J. Membr. Sci.* **2021**, *618*, 118657. [CrossRef]
32. Golovanova, A.V.; Domnina, M.A.; Arzhanov, A.I.; Karimullin, K.R.; Eremchev, I.Y.; Naumov, A.V. AFM Characterization of Track-Etched Membranes: Pores Parameters Distribution and Disorder Factor. *Appl. Sci.* **2022**, *12*, 1334. [CrossRef]
33. Yamaki, T.; Nuryanthi, N.; Kitamura, A.; Koshikawa, H.; Sawada, S.; Voss, K.-O.; Severin, D.; Trautman, C. Fluoropoly-mer-based nanostructured membranes created by swift-heavy-ion irradiation and their energy and environmental applications. *Nucl. Instrum. Methods Phys. Res. Sect. B* **2018**, *435*, 162–168. [CrossRef]
34. Dauletbekova, A.; Vlasukova, L.; Baimukhanov, Z.; Akilbekov, A.; Kozlovskiy, A.; Giniyatova, S.H.; Seitbayev, A.; Usseinov, A.; Akylbekova, A. Synthesis of ZnO nanocrystals in SiO_2/Si track template: Effect of electrodeposition parameters on structure. *Physica Stat Solidi B* **2019**, *256*, 1800408. [CrossRef]
35. Giniyatova, S.; Dauletbekova, A.; Baimukhanov, Z.; Vlasukova, L.; Akilbekov, A.; Usseinov, A.; Kozlovskiy, A.; Akylbekova, A. Structure, electrical properties and luminescence of ZnO nanocrystals deposited in SiO_2/Si track templates. *Radiat. Meas.* **2019**, *125*, 52–56. [CrossRef]
36. Balakhayeva, R.; Akilbekov, A.; Baimukhanov, Z.; Usseinov, A.; Giniyatova, S.; Zdorovets, M.; Vlasukova, L.; Popov, A.I.; Dauletbekova, A. CdTe Nanocrystal Synthesis in SiO_2/Si Ion-Track Template: The Study of Electronic and Structural Properties. *Phys. Status Solidi A* **2021**, *218*, 2000231. [CrossRef]
37. Akilbekov, A.; Balakhayeva, R.; Zdorovets, M.; Baymukhanov, Z.; Komarov, F.F.; Karim, K.; Popov, A.I.; Dauletbekova, A. Ion track template technology for fabrication of CdTe and CdO nanocrystals. *Nucl. Inst. Methods Phys. Res. B* **2020**, *481*, 30–34. [CrossRef]
38. Balakhayeva, R.; Akilbekov, A.; Baimukhanov, Z.; Giniyatova, S.; Zdorovets, M.; Gorin, Y.; Popov, A.I.; Dauletbekova, A. Structure properties of CdTe nanocrystals created in SiO_2/Si ion track Templates. *Surf. Coat. Technol.* **2020**, *401*, 126269. [CrossRef]
39. Ivanou, D.K.; Streltsov, E.A.; Fedotov, A.K.; Mazanik, A.V.; Fink, D.; Petrov, A. Electrochemical deposition of PbSe and CdTe nanoparticles onto p-Si(100) wafers and into nanopores in SiO_2/Si(100) structure. *Thin Solid Films* **2005**, *490*, 154–160. [CrossRef]
40. Akilbekov, A.; Akylbekova, A.; Usseinov, A.; Kozlovskyi, A.; Baymukhanov, Z.; Giniyatova, S.; Popov, A.I.; Dauletbekova, A. Ion track template technique for fabrication of $ZnSe_2O_5$ nanocrystals. *Nuclear Instrum. Methods Phys. Res. B* **2020**, *476*, 10–13. [CrossRef]
41. Akylbekova, A.; Dauletbekova, A.; Baymukhanov, Z.; Kozlovsky, A.; Usseinov, A. Template synthesis of $ZnSe_2O_5$ nanocrystals. *AIP Conf. Proc.* **2019**, *2174*, 020001.
42. Kaniukov, E.; Yakimchuk, D.; Arzumanyan, G.; Terryn, H.; Baert, K.; Kozlovskiy, A.; Zdorovets, M.; Belonogov, E.; Demyanov, S. Growth mechanisms of spatially separated copper dendrites in pores of a SiO_2 template. *Philos. Mag.* **2017**, *97*, 2268–2283. [CrossRef]
43. Demyanov, E.; Kaniukov, Y.E.; Petrov, A.V.; Belonogov, E.K.; Streltsov, E.A.; Ivanov, D.K.; Ivanova, Y.A.; Trautmann, C.; Terryn, H.; Petrova, M.; et al. On the morphology of Si/SiO_2/Ni nanostructures with swift heavy ion tracks in silicon oxide. *J. Surf. Investig.* **2014**, *8*, 805–813. [CrossRef]
44. Bundyukova, V.D. Porous SiO_2/Si templates for the formation of plasmon nanostructures. In Proceedings of the Women scientists of Belarus and Kazakhstan: Materials of the International Scientific-Practical Conference, Minsk, Belarus, 1–2 March 2018; pp. 463–465. Available online: http://elib.bsu.by/handle/123456789/196112 (accessed on 25 February 2022).
45. Bundyukova, V.D.; Yakimchuk, D.V.; Kaniukov, E.Y.; Tishkevich, D.I.; Kutuzau, M.D.; Prigodich, V.V.; Shemukhin, A.A.; Balakshin, Y.V.; Nazarov, A.V.; Kozhemiako, A.V.; et al. Modification of an SiO_2(Au)/Si Surface by Irradiation with Argon Ions. *Mosc. Univ. Phys. Bull.* **2020**, *75*, 225–229. [CrossRef]
46. Ashrafia, A.; Jagadish, C. Review of zincblende ZnO: Stability of metastable ZnO phases. *J. Appl. Phys* **2007**, *102*, 071101. [CrossRef]

47. Uklein, A.; Multian, V.; Kuz'micheva, G.; Linnik, R.; Lisnyak, V.; Popov, A.; Gayvoronsky, V.Y. Nonlinear optical response of bulk ZnO crystals with different content of intrinsic defects. *Opt. Mater.* **2018**, *84*, 738–747. [CrossRef]
48. Pashkevich, A.V.; Fedotov, A.K.; Poddenezhny, E.N.; Bliznyuk, L.A.; Fedotova, J.A.; Basov, N.A.; Kharchanka, A.A.; Zukowski, P.; Koltunowicz, T.N.; Korolik, O.V.; et al. Structure, electric and thermoelectric properties of binary ZnO-based ceramics doped with Fe and Co. *J. Alloys Compd.* **2022**, *895*, 162621. [CrossRef]
49. Karbovnyk, I.; Sadoviy, B.; Turko, B.; Kostruba, A.M.; Luchechko, A.; Vasil'yev, V.S.; Kukhta, A.V. Optical properties of composite structure based on ZnO microneedles and Alq3 thin film. *Opt. Quantum Electron.* **2021**, *53*, 647. [CrossRef]
50. Ostanina, T.N.; Rudoi, V.M.; Nikitin, V.S.; Darintseva, A.B.; Zalesova, O.L.; Porotnikova, N.M. Determination of the surface of dendritic electrolytic zinc powders and evaluation of its fractal dimension. *Russ. J. Non-Ferr. Met.* **2016**, *57*, 47–51. [CrossRef]
51. Khaliullin, S.M.; Zhuravlev, V.D.; Ermakova, L.V.; Buldakova, L.Y.; Yanchenko, M.Y.; Porotnikova, N.M. Solution combustion synthesis of ZnO using binary fuel (glycine+ citric acid). *Int. J. Self-Propagating High-Temp. Synth.* **2019**, *28*, 226–232. [CrossRef]
52. Borade, P.A.; Sant, T.; Gokarna, A.; Joshi, K.U.; Panat, R.P.; Jejurikar, S.M. Role of defects in modulating the near band edge emissions of sub-micron ZnO crystals. *Opt. Mater.* **2020**, *109*, 110348. [CrossRef]
53. Rout, A.; Boltaev, G.S.; Ganeev, R.A.; Rao, K.S.; Fu, D.; Rakhimov, R.Y.; Kurbanov, S.S.; Urolov, S.Z.; Shaymardanov, Z.S.; Guo, C.; et al. Low-and high-order nonlinear optical studies of ZnO nanocrystals, nanoparticles, and nanorods. *Eur. Phys. J. D* **2019**, *73*, 235. [CrossRef]
54. Sharopov, U.B.; Atabaev, B.G.; Djabbarganov, R. Defect Formation on the Surface of ZnO Using Low-Energy Electrons. *J. Surf. Investig. X-Ray Synchrotron Neutron Tech.* **2020**, *14*, 101–104. [CrossRef]
55. El Filali, B.; Gomez, J.J.; Torchynska, T.V.; Espinola, J.C.; Shcherbyna, L. Band-edge emission, defects, morphology and structure of in-doped ZnO nanocrystal films. *Opt. Mater.* **2019**, *89*, 322–328. [CrossRef]
56. Lin, Y.-P.; Polyakov, B.; Butanovs, E.; Popov, A.A.; Sokolov, M.; Bocharov, D.; Piskunov, S. Excited States Calculations of MoS2@ZnO and WS2@ZnO Two-Dimensional Nanocomposites for Water-Splitting Applications. *Energies* **2022**, *15*, 150. [CrossRef]
57. Spataro, G.; Champouret, Y.; Florian, P.; Coppel, Y.; Kahn, M.L. Multinuclear solid-state NMR study: A powerful tool for understanding the structure of ZnO hybrid nanoparticles. *Phys. Chem. Chem. Phys.* **2018**, *20*, 12413–12421. [CrossRef]
58. Jońca, J.; Ryzhikov, A.; Kahn, M.L.; Fajerwerg, K.; Chaudret, B.; Chapelle, A.; Fau, P. Shape-controlled ZnO nanostructures for gas sensing applications. *Procedia Eng.* **2014**, *87*, 907–910. [CrossRef]
59. Saliba, S.; Coppel, Y.; Davidson, P.; Mingotaud, C.; Chaudret, B.; Kahn, M.L.; Marty, J.D. Liquid crystal based on hybrid zinc oxide nanoparticles. *J. Mater. Chem.* **2011**, *21*, 6821–6823. [CrossRef]
60. Carrey, J.; Carrere, H.; Kahn, M.L.; Chaudret, B.; Marie, X.; Respaud, M. Photoconductivity of self-assembled ZnO nanoparticles synthesized by organometallic chemistry. *Semicond. Sci. Technol.* **2007**, *23*, 025003. [CrossRef]
61. Moorthy, S.; Moorthy, G.; Swaminathan, K. Fabrication of Novel $ZnSeO_3$ Anchored on g-C_3N_4 Nanosheets: An Outstanding Photocatalyst for the Mitigation of Pesticides and Pharmaceuticals. *J. Inorg. Organomet. Polym. Mater.* **2020**, *30*, 4664–4676. [CrossRef]
62. Hassan, S.A.; Bashir, S.; Zehra, K.; Ahmed, Q.S. Structural, morphological and optical properties of pulsed laser deposited ZnSe/$ZnSeO_3$ thin films. *Mater. Res. Express* **2018**, *5*, 046404. [CrossRef]
63. Jiang, H.Q.; Jun, C.H.E.; Li, Z.M.; Xi, Y.A.O. A reduction approach to prepare ZnSe nanocrystallites. *Trans. Nonferrous Met. Soc. China* **2006**, *16*, s419–s422. [CrossRef]
64. Al'zhanova, A.; Dauletbekova, A.; Komarov, F.; Vlasukova, L.; Yuvchenko, V.; Akilbekov, A.; Zdorovets, M. Peculiarities of latent track etching in SiO_2/Si structures irradiated with Ar, Kr and Xe ions. *Nucl. Instrum. Methods Phys. Res. Sect. B Beam Interact. Mater. At.* **2016**, *374*, 121–124. [CrossRef]
65. Vlasukova, L.; Komarov, F.; Yuvchenko, V.; Baran, L.; Milchanin, O.; Dauletbekova, A.; Alzhanova, A.; Akilbekov, A. Etching of latent tracks in amorphous SiO_2 and Si_3N_4: Simulation and experiment. *Vacuum* **2016**, *129*, 137–141. [CrossRef]
66. Studenikin, S.A.; Golego, N.; Cocivera, M. Fabrication of green and orange photoluminescent, undoped ZnO films using spray pyrolysis. *J. Appl. Phys.* **1998**, *84*, 2287–2294. [CrossRef]
67. Degoda, V.Y.; Sofienko, A.O. Specific features of the luminescence and conductivity of zinc selenide on exposure to X-ray and optical excitation. *Semiconductors* **2010**, *44*, 568–574. [CrossRef]
68. Degoda, V.Y.; Podust, G.P.; Doroshenko, I.Y.; Pavlova, N.Y. Phosphorescence and conduction current relaxation in ZnSe crystals. *Opt. Mater.* **2022**, *129*, 112460. [CrossRef]
69. Perdew, P.; Burke, K.; Ernzerhof, M. Generalized Gradient Approximation Made Simple. *Phys. Rev. Lett.* **1996**, *77*, 3865–3868. [CrossRef]
70. Dovesi, R.; Saunders, V.R.; Roetti, R.; Orlando, R.; Zicovich-Wilson, C.M.; Pascale, F.; Civalleri, B.; Doll, K.; Harrison, N.M.; Bush, I.J.; et al. CRYSTAL14 User's Manual University of Torino, Italy. Available online: http://www.crystal.unito.it. (accessed on 4 February 2022).
71. Jaffe, J.E.; Hess, A.C. Hartree-Fock study of phase changes in ZnO at high pressure. *Phys. Rev. B* **1993**, *48*, 7903–7909. [CrossRef]
72. Towler, M.D.; Zicovich-Wilson, C. Selenium Basis Set for the Crystal Program. Available online: https://vallico.net/mike_towler//basis_sets/Se_basis.txt (accessed on 4 March 2019).
73. Gallino, G.; Pacchioni, C.; Valentin, D. Transition levels of defect centers in ZnO by hybrid functionals and localized basis set approach. *J. Chem. Phys* **2010**, *133*, 144512. [CrossRef]

74. Van de Walle, C.G.; Neugebauer, J. First-principles calculations for defects and impurities: Applications to III-nitrides. *J. Appl. Phys.* **2004**, *95*, 3851–3879. [CrossRef]
75. Mulliken, R.S. Electronic population analysis on LCAO-MO molecular wave functions. *J. Chem. Phys.* **1955**, *23*, 1833–1840. [CrossRef]
76. Kohn, K.; Inoue, K.; Horie, O.; Akimoto, S. Crystal Chemistry of $MSeO_3$ and $MTeO_3$, (M = Mg, Mn, Co, Ni, Cu, and Zn). *J. Solid State Chem.* **1976**, *18*, 27–37. [CrossRef]